

Power Spectrum Emulators from Neural Networks and Tree-Based Methods

Andrei Lazanu

Department of Physics and Astronomy, University of Manchester, Manchester M13 9PL, United Kingdom

E-mail: andrei.lazanu@manchester.ac.uk

Abstract. We use two subsets of 2000 and 1000 QUIJOTE simulations to build two power spectrum emulators, allowing for fast computations of the non-linear matter power spectrum. The first emulator works on scales $k \in [0.015, 1.8] h/\text{Mpc}^{-1}$ in terms of seven cosmological parameters: the matter and baryon fraction of the energy density of the Universe Ω_m and Ω_b , the reduced Hubble constant h , the scalar spectral index n_s , the amplitude of matter density fluctuations σ_8 , the total neutrino mass M_ν and the dark energy equation of state parameter w . The power spectra can be directly determined at redshifts 0, 0.5, 1, 2 and 3, while for intermediate redshifts these can be interpolated. The second emulator is based on five cosmological parameters, Ω_m , h , n_s , σ_8 and the amplitude of equilateral non-Gaussianity $f_{\text{NL}}^{\text{equilateral}}$, at redshifts 0, 0.503, 0.733, 0.997 for $k \in [0.015, 1.8] h/\text{Mpc}^{-1}$. The emulators are built on machine learning techniques. In both cases we have investigated both neural networks and tree-based methods and we have shown that the best accuracy is obtained for a neural network with two hidden layers. Both emulators achieve a root-mean-squared relative error of less than 5% for all the redshifts considered on the scales discussed.

Contents

1	Introduction	1
2	ΛCDM extensions	2
2.1	Massive neutrinos and dark energy equation of state parameter	2
2.2	Equilateral primordial non-Gaussianity	3
3	Numerical simulations and methodology	3
4	Results for neutrinos and dark energy equation of state parameter	4
5	Results for primordial non-Gaussianity	7
6	Discussion, conclusions and future directions	8

1 Introduction

Cosmology has become in the last few decades a precision science, mainly due to the unprecedented development of instruments capable of making cosmological measurements with exquisite accuracy. In particular, the Λ CDM model [1], a six-parameter model based on the spontaneous generation of primordial quantum fluctuations followed by an early-time inflationary epoch has been shown to accurately describe the cosmological observations from the Cosmic Microwave Background (CMB) data provided by COBE, WMAP [2], *Planck* [3], the Atacama Cosmology Telescope [4–7] and the South Pole Telescope [8, 9]. These have placed increasingly stringent constraints on the parameters of this model, as well as on its extensions. These constraints will become even tighter in the future, with observations from CMB-S4 [10] and the Simons Observatory [11].

In parallel, the late-time matter and galaxy distributions, the large-scale-structure (LSS), can provide complementary information to the CMB, with valuable information coming from its three-dimensional nature given by the redshift, in addition to the distribution of galaxies on the sky. Current LSS probes, such as the Dark Energy Survey [12], the Kilo-Degree Survey [13], as well as experiments in progress, and future ones, such as Euclid [14], the Vera C. Rubin Observatory Legacy Survey of Space and Time [15], the Square Kilometre Array [16], the Nancy Grace Roman Space Telescope [17] will be able to improve our understanding even further. The exquisite accuracy in the measurements of these experiments must be matched by the theoretical modelling.

However, modelling of non-linear scales remains a challenge: perturbation theories break down at a certain scale, and one has to rely on phenomenological models, fit on simulations or work directly with the desired simulations. In recent years, a large number of simulations have been produced, and their generation and processing has benefited from important progress in machine learning usage. Machine learning has been used in a large number of fields in cosmology, including CMB [18, 19], LSS [20–23], reionization and 21cm [24–27], gravitational lensing: weak lensing [28, 29], strong lensing [30, 31], redshift prediction [32, 33], parameter estimation [34–36] etc.

In spite of the significant advances in computational power, these remain expensive to run and phenomenological models rely on specific simulations; new simulations, or simulations taking into account additional parameters can require a complete rethink of the model. Hence, emulators have been built to mitigate these issues. These are particularly useful where a specific cosmological quantity (such as the power spectrum in this work) needs to be repeatedly calculated, for example, in the case of placing parameter constraints using Markov-Chain-Monte-Carlo (MCMC) methods. The techniques employed to build such quantities are varied and have started with the pioneering fitting formulae, such as HALOFIT and its extensions [37–39], work involving Bayesian likelihood estimators, linear algebra data reduction techniques (such as Principal component analysis) and MCMC methods [40–46], to the use of Gaussian processes [47–51] and neural networks methods [52–67] and a combinations of analytical and numerical fits to the data [68–72]. These methods rely on a large number of simulations and the power spectra involve both Λ CDM cosmology and its extensions, such as modified gravity or massive neutrinos.

In this paper, we show how to build two emulators for the non-linear matter power spectrum, by using machine learning techniques starting from N -body simulations. The first one is based on simulations where seven cosmological parameters are varied: the dark matter density parameter Ω_m , the baryon density parameter Ω_b , the reduced Hubble constant h , the scalar spectral index n_s , the amplitude of the root-mean-square matter fluctuation averaged over a sphere of radius at $8h^{-1}\text{Mpc}$ σ_8 , the sum of the neutrino masses M_ν and the equation of state parameter for dark energy w .

The second emulator varies five cosmological parameters, Ω_m , h , n_s , σ_8 and the amplitude of equilateral primordial non-Gaussianity $f_{\text{NL}}^{\text{equilateral}}$. $\Omega_b = 0.049$ is fixed for these runs.

The paper is structured as follows: in Section 2 we briefly describe the two extensions to Λ CDM considered in this work, in Section 3 we present the simulations used in this work and the machine learning models employed in the analysis; Section 4 presents our results from the fittings and the performances of each of the seven-parameter emulator which involves neutrino masses and the dark energy equation of state parameter, and Section 5 is devoted to the results for the emulator involving equilateral primordial non-Gaussianity; we conclude in Section 6.

2 Λ CDM extensions

2.1 Massive neutrinos and dark energy equation of state parameter

Neutrinos appear as a triplet and the oscillation experiments have confirmed that at least two types have non-zero masses [73]. Cosmological probes can constrain the sum of the neutrino masses – CMB constraints yield [74] $M_\nu = \Sigma m_\nu \lesssim 0.12\text{ eV}$ at 95% confidence level, while LSS can further constrain this further, to [75] $M_\nu \lesssim 0.0642\text{ eV}$.

The late-time cosmic acceleration, which has been experimentally observed [76] can be accounted for by the presence of dark energy. Its equation of state parameter, w , defined as the ratio between the pressure and the density of dark energy, quantifies how the Universe is expanding. The current constraints from the CMB [74] and LSS [77] are given by $w = -1.028 \pm 0.031$ and $w = -0.99_{-0.13}^{+0.15}$ respectively. Both these measurements are compatible with $w = -1$, which corresponds to the cosmological constant. Hence, values $w \neq -1$, could point out to new physics beyond Λ CDM.

2.2 Equilateral primordial non-Gaussianity

Although the Λ CDM model is based on Gaussian scale-invariant primordial quantum fluctuations, most inflationary models predict some level of non-Gaussianity, which appears through a three-point function (bispectrum) correction at the primordial level. Indeed, for purely Gaussian fields, the two-point correlation function contains all the relevant information, and the bispectrum vanishes. The non-vanishing primordial bispectrum modifies the spectra throughout the history of the Universe, and in particular it has a contribution at the power spectrum level. As the bispectrum is three-dimensional (defined in Fourier space by the magnitudes of three wavevectors forming a triangle), its shape and amplitude (f_{NL}) both play important roles in the behaviour of cosmological quantities. Based on the details of the inflationary model considered, it peaks at various triangular configurations (see [78] for a review). These shapes, the most popular being the local, equilateral and orthogonal, have been tightly constrained by current CMB data from *Planck* [79], and in the future LSS surveys have the potential to tighten the constraints even further [80, 81]. Their effects can be measured through the power spectrum and from higher-order correlation functions.

In this paper, we focus on the equilateral type of non-Gaussianity; the primordial bispectrum B_{Φ}^{equil} can be expressed in terms of the primordial power spectrum P_{Φ} as

$$B_{\Phi}^{\text{equilateral}}(k_1, k_2, k_3) = 6 \{ -[P_{\Phi}(k_1)P_{\Phi}(k_2) + 2 \text{ perms}] - 2[P_{\Phi}(k_1)P_{\Phi}(k_2)P_{\Phi}(k_3)]^{2/3} + [P_{\Phi}^{1/3}(k_1)P_{\Phi}^{2/3}(k_2)P_{\Phi}(k_3) + 5 \text{ perms}] \} , \quad (2.1)$$

and $f_{\text{NL}}^{\text{equilateral}}$ represents the amplitude of this quantity. Experiments measure the amplitude of this shape, with current constraints given by $f_{\text{NL}}^{\text{equilateral}} = 6 \pm 46$. The detection of a non-zero equilateral-type of non-Gaussianity would point out to specific inflationary models, and in particular to single-field inflation with non-standard kinetic terms.

3 Numerical simulations and methodology

We built the emulators using a subset of the QUIJOTE simulations [82], a public suite of 88000 full N -body simulations, specifically run to quantify the information content on cosmological observables and to provide enough statistics to train machine learning algorithms. They have been run using the TreePM code Gadget-III [83] in boxes of sides of 1 Gpc/ h .

For the first emulator, we made use of a subset of 2000 simulations where seven cosmological parameters are varied, namely Ω_m , Ω_b , h , n_s , σ_8 , M_{ν} and w . They have been chosen using a latin-hypercube sampling method, a statistical method built for generating a near-random sample of parameter values from a multidimensional distribution [84]. The parameter ranges are given by: $\Omega_m \in [0.1, 0.5]$, $\Omega_b \in [0.03, 0.07]$, $h \in [0.5, 0.9]$, $n_s \in [0.8, 1.2]$, $\sigma_8 \in [0.6, 1]$, $M_{\nu} \in [0.01, 1.0] \text{ eV}$ and $w \in [-1.3, -0.7]$. The input power spectrum and transfer functions are set at $z = 127$ and have been obtained by rescaling the corresponding quantities derived at $z = 0$ from CAMB [85] using a method from Ref. [86], while the initial conditions have been generated using the Zel'dovich approximation.

The simulations have a volume of $1 (h^{-1} \text{Gpc})^3$ and contain 512^3 dark matter particles. Outputs are provided at redshifts 0, 0.5, 1, 2, 3 and in this study we use all of them. Several cosmological quantities are calculated from the simulations, but in this work we only focus on the matter power spectra.

The QUIJOTE simulations involving primordial non-Gaussianity [87, 88], are represented by a suite of 1000 simulations, where five parameters are sampled from a latin-hypercube,

with $\Omega_m \in [0.1, 0.5]$, $h \in [0.5, 0.9]$, $n_s \in [0.8, 1.2]$, $\sigma_8 \in [0.6, 1]$ and $f_{\text{NL}}^{\text{equilateral}} \in [-600, 600]$. The other cosmological parameters are fixed to $\Omega_b = 0.049$, $M_\nu = 0$ and $w = -1$. For these, the initial conditions for displacements and peculiar velocities are generated using second order perturbation theory, which in turn are used to assign to particles that are initially laid on a regular grid with the 2LPT code [89, 90]. In this case, snapshots are provided at four redshifts: 0, 0.503, 0.733, 0.997.

We investigated different learning models for building our emulator, including deep neural networks and tree-based methods. We also checked whether the performance of the models can be improved by reducing the target size with data-reduction techniques, such as principal component analysis (PCA) [91]. PCA consists of linearly transforming the data into a new orthogonal coordinate system such that the directions (principal components) that capture the largest variation in the data are ranked from highest to lowest. By keeping only a limited number of principal components, one can then reconstruct an approximation of the initial data matrix, at the same time keeping a controlled amount of the total variance of the data.

We also considered several tree-based methods to solve this regression problem, in particular Random Forests, and the gradient boosting techniques CatBoost [92], XGBoost [93] and LightGBM [94] and we compared the results of these methods with the ones of the neural networks.

Apart from the overall root mean squared error determined by the optimizers, in order to see how the models perform at each scale, we have computed the root-mean-squared-relative error (RMSRE) for the test set for each value k , defined as

$$\text{RMSRE}(k) = \sqrt{\frac{1}{n_{\text{test}}} \sum_{i \in \text{test set}} \left(\frac{P_{\text{emulator}}(k; \theta_i)}{P_{\text{simulation}}(k; \theta_i)} - 1 \right)^2}, \quad (3.1)$$

for each of the models considered, where θ_i represents the parameter vector of the i th power spectrum of the test set and n_{test} represents the size of the test set. For a good modelling of the simulations by our emulator, this quantity must be as close to 0 as possible for all the scales considered.

For each of the tree-type models investigated, we have considered randomized cross-validation for some of the hyperparameters to see if any improvement can be gained.

4 Results for neutrinos and dark energy equation of state parameter

In order to build the emulator, we trained learning models on the input data, consisting of the seven cosmological parameters varied in the simulations, while the output (target) variables are given by the corresponding power spectra, at fixed values of the wavevector $k \in [0.008900, 2.785996] h/\text{Mpc}$. As at large scales errors are expected to be large due to cosmic variance and at low scales the accuracy of the simulations is limited due to the resolution considered, we restrict the k -range to $k \in [0.015, 1.80] h/\text{Mpc}$ for the training and predictions. Due to the limited redshift values available from the simulations, we chose not to use z as an additional feature of the model, and we build separate models for each redshift showing how one can potentially interpolate between them.

The inputs are linearly scaled so that they are all in the interval $[0, 1]$. The outputs are represented by the matter power spectra, evaluated at fixed values of k . As the power spectra span several orders of magnitude at each redshift, $P(k) \in (10^2, 10^5)$ at $z = 0$ to $(1, 10^4)$ at

$z = 3$, we apply logarithms in order to make all values $\mathcal{O}(1)$. We started by randomly splitting the 2000 simulations into a training set and a test set. In order to improve the performance of the model by having a large enough training set, we only separated 100 simulations for testing purposes. For the methods considered, we have implemented two scenarios: one using the full output for the scales considered, in 285 points (k -values), and a compressed version of 11 points using PCA. In this case, more than 99.5% of the variance of the matrix of power spectra is preserved.

For neural networks, several architectures have been investigated, and the best performing one consists of two hidden layers. For the full power spectrum output, the input vector consists of the seven features; there are two hidden layers with 2048 neurons each, with ReLU activation functions, followed by Dropout layers with rates of 15% (15% of the nodes are randomly set to 0 at each iteration), while for the 285 targets a linear activation layer has been applied. A mean-squared-error loss function and an Adam optimizer with a rate of 10^{-4} have been used. In order to perform the optimisation, and to split the data into training and validation sets, a K-fold splitting has been introduced with $k = 5$. This technique increases the predictive power of the model, by splitting the training set into k folds, each of which is used as a validation set and the model is trained k times. Thus, $k = 5$ models were run, and their predictions on the test set were averaged, yielding the final answer. 3000 training steps were set for each of the runs, but early stopping was also implemented, watching the decrease of the validation loss. Both the Dropout layers and early stopping were implemented to avoid overfitting.

A similar network architecture has been considered for the PCA output, with the same hidden layer sizes, but the Dropout rate has been set to 60%. We note that here, in order to avoid data leakage, the PCA transformation matrix has been obtained from the training set in each of the k -folds, and the same transformation has been used on the validation and test sets too. Finally, the reconstruction of the power spectrum was performed using the inverse transformation from each of the k -folds.

The overall training time of each of these two networks was around 15 minutes on a NVIDIA Tesla T4 GPU with 40 cores.

In the case of tree-based methods, we have considered the models described in Section 3, with the RMSRE plotted in Fig. 1. We noticed that, despite our best efforts, XGBoost and LightGBM are not producing satisfactory results, and hence we only worked with the neural networks and with CatBoost for the other redshifts. Moreover, modifying the CatBoost parameters does not seem to improve the performance of the model, with the exception of increasing the number of iterations, which also peaks around the value considered. The full CatBoost model runs for around 30 minutes with 5000 iterations on a single core, whereas for the PCA version the runtime is around 5 minutes with the same number of iterations.

The figure shows that the models involving the neural network are the best performing, with the PCA having a slightly better score. This is most likely due to the fact that the network has a significantly easier job of training on a reduced output. The RMSRE for these models is below 3% for $k > 0.15h/\text{Mpc}$ models and below 5% for $0.10h/\text{Mpc} < k < 0.15h/\text{Mpc}$. The performance is decreasing significantly for lower values of k , mainly due to the noise in the simulations. At these scales, cosmic variance is important, and the sample size is too low to compensate for it. CatBoost performs slightly worse, with a decrease of the RMSRE less than 1% to the neural networks for the scales of interest. The overall RMSEs for the 4 best models for the redshifts considered are presented in Table 1. These values are calculated on the power spectra (after applying the inverse PCA transform and

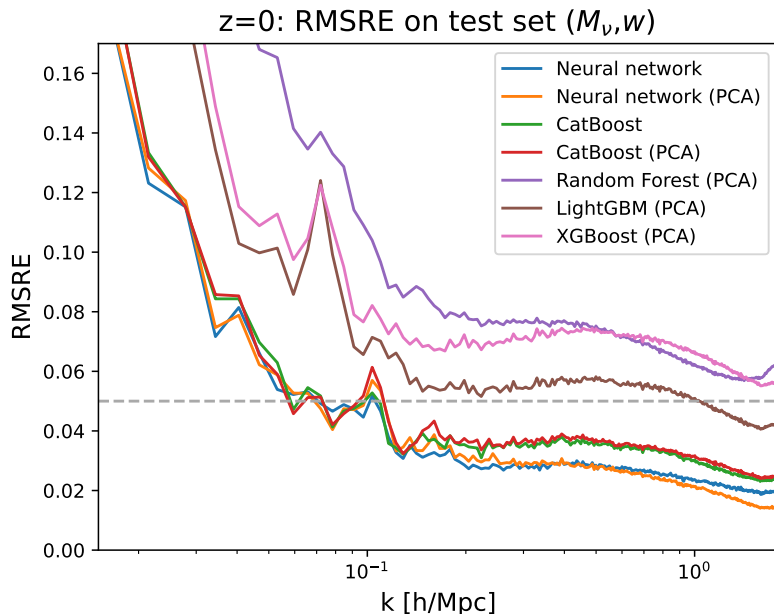


Figure 1. Comparison of RMSRE as a function of k on the test set for the seven-parameter emulator (Ω_m , Ω_b , h , n_s , σ_8 , M_ν and w) for the different learning models considered at $z = 0$.

exponentiating), which explains the larger values at lower redshifts.

Network	$z = 0$	$z=0.5$	$z = 1$	$z = 2$	$z = 3$
Neural network	430.8	295.5	210.1	95.7	56.9
Neural network (PCA)	358.4	219.9	166.6	84.7	47.0
CatBoost	555.9	392.6	257.1	134.3	74.5
CatBoost (PCA)	582.1	380.0	268.9	130.5	70.1

Table 1. The RMSE for the 4 best models considered at the redshifts of the simulations (0, 0.5, 1, 2 and 3) for the emulator with seven cosmological parameters: Ω_m , Ω_b , h , n_s , σ_8 , M_ν and w .

As the neural network involving the PCA with 11 principal components systematically produces the best RMSRE, we only plot that for clarity at all redshifts, with the results shown in Fig. 2.

Due to the limited number of redshift snapshots available, we could not run inference models on the data. However, we know that for linear theory, the power spectrum can be expressed in terms of the growth rate $D(z)$ as $P_{\text{lin}}(k, z) = D^2(z)P_{\text{lin}}(k, 0)$, where $D(z = 0) = 1$. This scaling function depends, of course, on the evolution history of the universe and hence on the cosmological parameters. However, one can see that $D^2(z)$ can be interpolated with a polynomial of degree 3 in redshift. Hence, for intermediate redshifts, we can use the outputs of the models for the 5 redshifts, and our emulator will output the interpolated values using least squares.

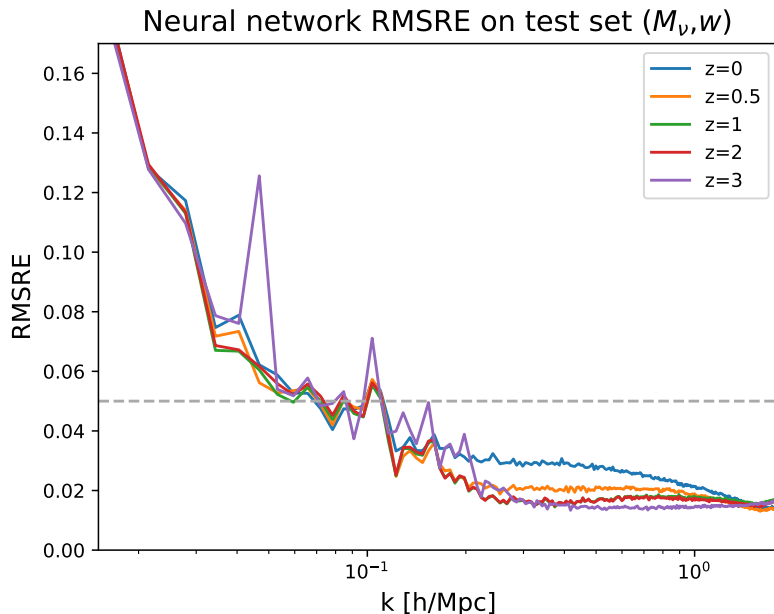


Figure 2. RMSRE for the neural network (with PCA) for redshifts 0, 0.5, 1, 2 and 3 for the emulator involving the sum of neutrino masses and the dark energy equation of state

5 Results for primordial non-Gaussianity

In this section we discuss the findings of the emulator involving $f_{\text{NL}}^{\text{equilateral}}$. In this case, there are five cosmological parameters that are varied, and hence the emulator will have 5-dimensional input data. The wavevector range is here $k \in [0.008900, 5, 569] \text{ h/Mpc}$ and we chose to restrict its range to $[0.015, 2.0] \text{ h/Mpc}$. In this simulations, there are only four redshifts for the snapshots, and therefore the third-order fit for intermediate redshifts will be less precise.

The number of simulations is 1000, and here we chose a random test set of size 100 to test the model. For convenience, we used a model architecture similar to the previous one, with two hidden layers for both the full power spectrum and the PCA versions, with the same number of neurons. In the case of the full power spectrum, there are 317 outputs, and for the PCA we again choose 11 principal components, which preserve 99.96% of the variance. A comparison at $z = 0$ of the RMSRE for the models considered shows that the Random forests, LightGBM and XGBoost perform much worse than the neural network and CatBoost by a few percent on the test set. The neural network results are similar for the non-PCA and PCA versions, which is also the case for CatBoost, which performs marginally worse than the neural networks. However, we note that, in the case of this method, using PCA compression significantly reduces the training time and requires less tuning than a neural network, where the choice of architecture is essential. The running times of these models were similar to those of the first emulator.

The trends observed at $z = 0$ are maintained at the other three redshifts as one can see from Table 2, where the overall RMSE has been calculated. Indeed, the neural network (PCA compressed) works best at all redshifts, while CatBoost is slightly worse, with the two

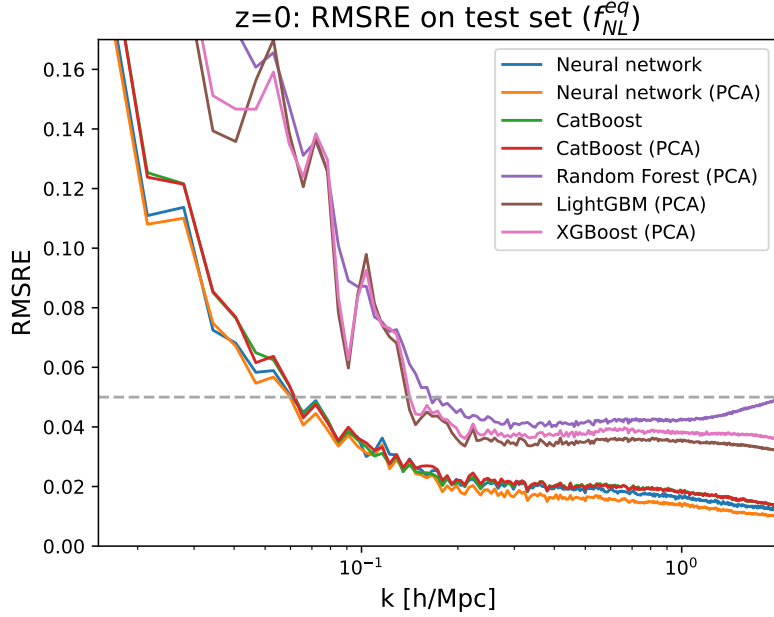


Figure 3. Comparison of RMSRE as a function of k on the test set for the five-parameter emulator involving equilateral non-Gaussianity for the different learning models considered.

versions (PCA and non-PCA) almost indistinguishable.

Network	$z = 0$	$z = 0.503$	$z = 0.733$	$z = 0.997$
Neural network	144.3	99.4	80.4	68.1
Neural network (PCA)	137.1	91.4	78.1	63.7
CatBoost	169.6	116.5	98.8	83.1
CatBoost (PCA)	169.0	116.7	99.4	81.1

Table 2. RMSEs for the 4 best models considered at the redshifts of the simulations (0, 0.503, 0.733, 0.997) for the emulator with five cosmological parameters: Ω_m , h , n_s , σ_8 and $f_{\text{NL}}^{\text{equilateral}}$.

To see the behaviour of the emulator at each scale, we again focussed on the best model – the PCA compressed neural network. We plot the RMSRE in terms of scale for this model at the four redshifts considered (Fig. 4), and we see that this metric is lower than 4% for $k > 0.1 h/\text{Mpc}$ and this drops to around 1% for $k \sim 2 h/\text{Mpc}$. For $k < 0.1 h/\text{Mpc}$, the results are not so accurate, due to the cosmic variance that has not been mitigated by running a large number of simulations.

6 Discussion, conclusions and future directions

In this work we have made the choice to look at the logarithm of the power spectrum from the simulation rather than consider the ratio of the model to the linear or some nonlinear (like HALOFIT) version of the matter power spectrum which has been used in the literature. This procedure has the advantage that it does not require external data, or running a Boltzmann code, to generate the linear or non-linear power spectrum.

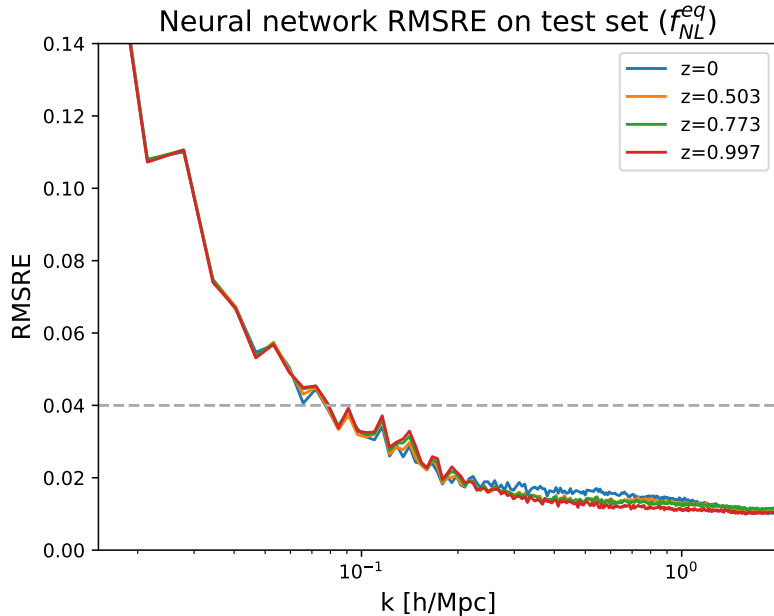


Figure 4. RMSRE for the neural network (with PCA) for redshifts 0, 0.503, 0.733 and 0.997 for the five-parameter emulator involving $f_{\text{NL}}^{\text{equilateral}}$.

We have shown how accurate N -body QUIJOTE simulations can be used to build power spectrum emulators for different cosmological parameters. In particular, we built two power spectrum emulators: one varying seven cosmological parameters, including the total sum of neutrino masses and the parameter describing the equation of state of dark energy, and a second one, varying five parameters including the amplitude of primordial equilateral non-Gaussianity.

For each of them we have investigated several machine learning models, including neural networks and tree-based methods. We have looked into methods to compress the power spectrum outputs and we showed that 11 principal components from PCA can encode more than 99.5% of the variance of the data.

In the case of the neural networks, the best performing model determined has an architecture with two 2048-neuron hidden layers with ReLU activation functions, followed by Dropout layers. The dropout rates are of 15% and 60% for the full and PCA versions respectively. For both emulators, the PCA neural network achieved better than 5% RMSRE for all the scales considered. In what concerns tree-based methods, we have investigated Random Forests, CatBoost XGBoost and LightGBM, showing that only CatBoost can provide competitive results to the neural networks, with RMSRE less than 1% worse than the them.

For intermediate redshifts, one can numerically interpolate using a third-order polynomial in redshifts.

The results that we have obtained here can be improved by significantly increasing the number of simulations used for training the networks. As emulators are powerful tools that can be used to replace simulations in situations where a large number of runs is required, we aim to investigate this area in more detail in future work, and in particular to look at different cosmological quantities, such as the bispectrum.

Acknowledgments

The author has been supported by a United Kingdom Research and Innovation (UKRI) Future Leaders Fellowship [Grant No. MR/V021974/2].

Data availability

The learning models are available as Jupyter notebooks on GitHub at https://github.com/andreilazanu/power_spectrum_emulators. The data from the QUIJOTE simulations is available on <https://quijote-simulations.readthedocs.io/en/latest/>, where detailed instructions are given on how to download and use the information available.

References

- [1] S. Weinberg, *The cosmological constant problem*, *Rev. Mod. Phys.* **61** (Jan, 1989) 1–23.
- [2] C. L. Bennett, M. Bay, M. Halpern, G. Hinshaw, C. Jackson, N. Jarosik et al., *The Microwave Anisotropy Probe Mission*, *Astrophys. J.* **583** (Jan., 2003) 1–23, [[astro-ph/0301158](#)].
- [3] PLANCK collaboration, N. Aghanim et al., *Planck 2018 results. I. Overview and the cosmological legacy of Planck*, *Astron. Astrophys.* **641** (2020) A1, [[1807.06205](#)].
- [4] ACT collaboration, S. Aiola et al., *The Atacama Cosmology Telescope: DR4 Maps and Cosmological Parameters*, *JCAP* **12** (2020) 047, [[2007.07288](#)].
- [5] ACT collaboration, S. K. Choi et al., *The Atacama Cosmology Telescope: a measurement of the Cosmic Microwave Background power spectra at 98 and 150 GHz*, *JCAP* **12** (2020) 045, [[2007.07289](#)].
- [6] ACT collaboration, M. S. Madhavacheril et al., *The Atacama Cosmology Telescope: DR6 Gravitational Lensing Map and Cosmological Parameters*, *Astrophys. J.* **962** (2024) 113, [[2304.05203](#)].
- [7] ACT collaboration, F. J. Qu et al., *The Atacama Cosmology Telescope: A Measurement of the DR6 CMB Lensing Power Spectrum and Its Implications for Structure Growth*, *Astrophys. J.* **962** (2024) 112, [[2304.05202](#)].
- [8] SPT-3G collaboration, L. Balkenhol et al., *Measurement of the CMB temperature power spectrum and constraints on cosmology from the SPT-3G 2018 TT, TE, and EE dataset*, *Phys. Rev. D* **108** (2023) 023510, [[2212.05642](#)].
- [9] SPT collaboration, Z. Pan et al., *Measurement of gravitational lensing of the cosmic microwave background using SPT-3G 2018 data*, *Phys. Rev. D* **108** (2023) 122005, [[2308.11608](#)].
- [10] CMB-S4 collaboration, K. N. Abazajian et al., *CMB-S4 Science Book, First Edition*, [1610.02743](#).
- [11] SIMONS OBSERVATORY collaboration, P. Ade et al., *The Simons Observatory: Science goals and forecasts*, *JCAP* **02** (2019) 056, [[1808.07445](#)].
- [12] DES collaboration, T. M. C. Abbott et al., *Dark Energy Survey Year 3 results: Cosmological constraints from galaxy clustering and weak lensing*, *Phys. Rev. D* **105** (2022) 023520, [[2105.13549](#)].
- [13] C. Heymans et al., *KiDS-1000 Cosmology: Multi-probe weak gravitational lensing and spectroscopic galaxy clustering constraints*, *Astron. Astrophys.* **646** (2021) A140, [[2007.15632](#)].
- [14] EUCLID collaboration, R. Laureijs et al., *Euclid Definition Study Report*, [1110.3193](#).

- [15] LSST SCIENCE, LSST PROJECT collaboration, P. A. Abell et al., *LSST Science Book, Version 2.0*, [0912.0201](#).
- [16] M. J. Jarvis, D. Bacon, C. Blake, M. L. Brown, S. N. Lindsay, A. Raccañelli et al., *Cosmology with SKA Radio Continuum Surveys*, [1501.03825](#).
- [17] T. Eifler et al., *Cosmology with the Roman Space Telescope – multiprobe strategies*, *Mon. Not. Roy. Astron. Soc.* **507** (2021) 1746–1761, [[2004.05271](#)].
- [18] J. a. Caldeira, W. L. K. Wu, B. Nord, C. Avestruz, S. Trivedi and K. T. Story, *DeepCMB: Lensing Reconstruction of the Cosmic Microwave Background with Deep Neural Networks*, *Astron. Comput.* **28** (2019) 100307, [[1810.01483](#)].
- [19] P. Chanda and R. Saha, *An Unbiased Estimator of the Full-sky CMB Angular Power Spectrum using Neural Networks*, [2102.04327](#).
- [20] A. C. Rodriguez, T. Kacprzak, A. Lucchi, A. Amara, R. Sgier, J. Fluri et al., *Fast cosmic web simulations with generative adversarial networks*, *Comput. Astrophys. Cosmol.* **5** (2018) 4, [[1801.09070](#)].
- [21] L. Lucie-Smith, H. V. Peiris, A. Pontzen, B. Nord and J. Thiyaalingam, *Deep learning insights into cosmological structure formation*, [2011.10577](#).
- [22] Z. Lin, N. Huang, C. Avestruz, W. L. K. Wu, S. Trivedi, J. Caldeira et al., *DeepSZ: Identification of Sunyaev-Zel’dovich Galaxy Clusters using Deep Learning*, [2102.13123](#).
- [23] X. Xu, S. Kumar, I. Zehavi and S. Contreras, *Predicting halo occupation and galaxy assembly bias with machine learning*, [2107.01223](#).
- [24] H. Shimabukuro and B. Semelin, *Analysing the 21 cm signal from the epoch of reionization with artificial neural networks*, *Mon. Not. Roy. Astron. Soc.* **468** (2017) 3869–3877, [[1701.07026](#)].
- [25] L. Huang, R. A. C. Croft and H. Arora, *Deep Forest: Neural Network reconstruction of the Lyman-alpha forest*, [2009.10673](#).
- [26] T. Flöss and P. D. Meerburg, *Improving constraints on primordial non-Gaussianity using neural network based reconstruction*, *JCAP* **02** (2024) 031, [[2305.07018](#)].
- [27] A. Saxena, P. D. Meerburg, C. Weniger, E. d. L. Acedo and W. Handley, *Simulation-based inference of the sky-averaged 21-cm signal from CD-EoR with REACH*, *RAS Tech. Instrum.* **3** (2024) 724–736, [[2403.14618](#)].
- [28] D. Ribli, B. A. Pataki and I. Csabai, *An improved cosmological parameter inference scheme motivated by deep learning*, *Nature Astron.* **3** (2019) 93–98, [[1806.05995](#)].
- [29] J. M. Zorrilla Matilla, M. Sharma, D. Hsu and Z. Haiman, *Interpreting deep learning models for weak lensing*, *Phys. Rev. D* **102** (2020) 123506, [[2007.06529](#)].
- [30] C. Jacobs, K. Glazebrook, T. Collett, A. More and C. McCarthy, *Finding strong lenses in CFHTLS using convolutional neural networks*, *Mon. Not. Roy. Astron. Soc.* **471** (2017) 167–181, [[1704.02744](#)].
- [31] LSST DARK ENERGY SCIENCE collaboration, J. W. Park, S. Wagner-Carena, S. Birrer, P. J. Marshall, J. Y.-Y. Lin and A. Roodman, *Large-Scale Gravitational Lens Modeling with Bayesian Neural Networks for Accurate and Precise Inference of the Hubble Constant*, *Astrophys. J.* **910** (2021) 39, [[2012.00042](#)].
- [32] A. A. Collister and O. Lahav, *ANNz: Estimating photometric redshifts using artificial neural networks*, *Publ. Astron. Soc. Pac.* **116** (2004) 345–351, [[astro-ph/0311058](#)].
- [33] M. Eriksen et al., *The PAU Survey: Photometric redshifts using transfer learning from simulations*, *Mon. Not. Roy. Astron. Soc.* **497** (2020) 4565–4579, [[2004.07979](#)].

- [34] J. Alsing, T. Charnock, S. Feeney and B. Wandelt, *Fast likelihood-free cosmology with neural density estimators and active learning*, *Mon. Not. Roy. Astron. Soc.* **488** (2019) 4440–4458, [[1903.00007](#)].
- [35] A. Kostić, J. Jasche, D. K. Ramanah and G. Lavaux, *Machine-driven searches for cosmological physics*, [2107.00657](#).
- [36] A. Lazanu, *Extracting cosmological parameters from N-body simulations using machine learning techniques*, *JCAP* **09** (2021) 039, [[2106.11061](#)].
- [37] VIRGO CONSORTIUM collaboration, R. E. Smith, J. A. Peacock, A. Jenkins, S. D. M. White, C. S. Frenk, F. R. Pearce et al., *Stable clustering, the halo model and nonlinear cosmological power spectra*, *Mon. Not. Roy. Astron. Soc.* **341** (2003) 1311, [[astro-ph/0207664](#)].
- [38] R. Takahashi, M. Sato, T. Nishimichi, A. Taruya and M. Oguri, *Revising the Halofit Model for the Nonlinear Matter Power Spectrum*, *Astrophys. J.* **761** (2012) 152, [[1208.2701](#)].
- [39] A. Mead, S. Brieden, T. Tröster and C. Heymans, *hmcode-2020: improved modelling of non-linear cosmological power spectra with baryonic feedback*, *Mon. Not. Roy. Astron. Soc.* **502** (2021) 1401–1422, [[2009.01858](#)].
- [40] S. Habib, K. Heitmann, D. Higdon, C. Nakhleh and B. Williams, *Cosmic Calibration: Constraints from the Matter Power Spectrum and the Cosmic Microwave Background*, *Phys. Rev. D* **76** (2007) 083503, [[astro-ph/0702348](#)].
- [41] K. Heitmann, D. Higdon, C. Nakhleh and S. Habib, *Cosmic Calibration*, *Astrophys. J. Lett.* **646** (2006) L1–L4, [[astro-ph/0606154](#)].
- [42] K. Heitmann, M. White, C. Wagner, S. Habib and D. Higdon, *The Coyote Universe I: Precision Determination of the Nonlinear Matter Power Spectrum*, *Astrophys. J.* **715** (2010) 104–121, [[0812.1052](#)].
- [43] K. Heitmann, D. Higdon, M. White, S. Habib, B. J. Williams and C. Wagner, *The Coyote Universe II: Cosmological Models and Precision Emulation of the Nonlinear Matter Power Spectrum*, *Astrophys. J.* **705** (2009) 156–174, [[0902.0429](#)].
- [44] E. Lawrence, K. Heitmann, M. White, D. Higdon, C. Wagner, S. Habib et al., *The Coyote Universe III: Simulation Suite and Precision Emulator for the Nonlinear Matter Power Spectrum*, *Astrophys. J.* **713** (2010) 1322–1331, [[0912.4490](#)].
- [45] K. Heitmann, E. Lawrence, J. Kwan, S. Habib and D. Higdon, *The Coyote Universe Extended: Precision Emulation of the Matter Power Spectrum*, *Astrophys. J.* **780** (2014) 111, [[1304.7849](#)].
- [46] EUCLID collaboration, M. Knabenhans et al., *Euclid preparation: IX. EuclidEmulator2 – power spectrum emulation with massive neutrinos and self-consistent dark energy perturbations*, *Mon. Not. Roy. Astron. Soc.* **505** (2021) 2840–2869, [[2010.11288](#)].
- [47] C. Arnold, B. Li, B. Giblin, J. Harnois-Déraps and Y.-C. Cai, *forge: the f(R)-gravity cosmic emulator project – I. Introduction and matter power spectrum emulator*, *Mon. Not. Roy. Astron. Soc.* **515** (2022) 4161–4175, [[2109.04984](#)].
- [48] K. R. Moran, K. Heitmann, E. Lawrence, S. Habib, D. Bingham, A. Upadhye et al., *The Mira–Titan Universe – IV. High-precision power spectrum emulation*, *Mon. Not. Roy. Astron. Soc.* **520** (2023) 3443–3458, [[2207.12345](#)].
- [49] I. n. Sáez-Casares, Y. Rasera and B. Li, *The e-MANTIS emulator: fast predictions of the non-linear matter power spectrum in f(R)CDM cosmology*, *Mon. Not. Roy. Astron. Soc.* **527** (2024) 7242–7262, [[2303.08899](#)].
- [50] M.-F. Ho, S. Bird, M. A. Fernandez and C. R. Shelton, *MF-Box: multifidelity and multiscale emulation for the matter power spectrum*, *Mon. Not. Roy. Astron. Soc.* **526** (2023) 2903–2919, [[2306.03144](#)].

- [51] S. Günther, L. Balkenhol, C. Fidler, A. R. Khalife, J. Lesgourgues, M. R. Mosbech et al., *OLÉ– Online Learning Emulation in Cosmology*, [2503.13183](#).
- [52] S. Agarwal, F. B. Abdalla, H. A. Feldman, O. Lahav and S. A. Thomas, *PkANN - I. Non-linear matter power spectrum interpolation through artificial neural networks*, *Mon. Not. Roy. Astron. Soc.* **424** (2012) 1409–1418, [[1203.1695](#)].
- [53] S. Agarwal, F. B. Abdalla, H. A. Feldman, O. Lahav and S. A. Thomas, *pkann – II. A non-linear matter power spectrum interpolator developed using artificial neural networks*, *Mon. Not. Roy. Astron. Soc.* **439** (2014) 2102–2121, [[1312.2101](#)].
- [54] D. K. Ramanah, T. Charnock, F. Villaescusa-Navarro and B. D. Wandelt, *Super-resolution emulator of cosmological simulations using deep physical models*, *Mon. Not. Roy. Astron. Soc.* **495** (2020) 4227, [[2001.05519](#)].
- [55] R. E. Angulo, M. Zennaro, S. Contreras, G. Aricò, M. Pellejero-Ibañez and J. Stücker, *The BACCO simulation project: exploiting the full power of large-scale structure for cosmology*, *Mon. Not. Roy. Astron. Soc.* **507** (2021) 5869–5881, [[2004.06245](#)].
- [56] LSST DARK ENERGY SCIENCE collaboration, N. Ramachandra, G. Valogiannis, M. Ishak and K. Heitmann, *Matter Power Spectrum Emulator for $f(R)$ Modified Gravity Cosmologies*, *Phys. Rev. D* **103** (2021) 123525, [[2010.00596](#)].
- [57] N. Kaushal, F. Villaescusa-Navarro, E. Giusarma, Y. Li, C. Hawry and M. Reyes, *NECOLA: Toward a Universal Field-level Cosmological Emulator*, *Astrophys. J.* **930** (2022) 115, [[2111.02441](#)].
- [58] D. Jamieson, Y. Li, R. A. de Oliveira, F. Villaescusa-Navarro, S. Ho and D. N. Spergel, *Field-level Neural Network Emulator for Cosmological N-body Simulations*, *Astrophys. J.* **952** (2023) 145, [[2206.04594](#)].
- [59] B. Bolliet, A. Spurio Mancini, J. C. Hill, M. Madhavacheril, H. T. Jense, E. Calabrese et al., *High-accuracy emulators for observables in Λ CDM, N_{eff} , $\Sigma m\nu$, and w cosmologies*, *Mon. Not. Roy. Astron. Soc.* **531** (2024) 1351–1370, [[2303.01591](#)].
- [60] D. Piras and A. Spurio Mancini, *CosmoPower-JAX: high-dimensional Bayesian inference with differentiable cosmological emulators*, [2305.06347](#).
- [61] M. Bonici, F. Bianchini and J. Ruiz-Zapatero, *Capse.jl: efficient and auto-differentiable CMB power spectra emulation*, [2307.14339](#).
- [62] R. Maunland, H. A. Winther and C.-Z. Ruan, *Sesame: A power spectrum emulator pipeline for beyond- Λ CDM models*, *Astron. Astrophys.* **685** (2024) A156, [[2309.13295](#)].
- [63] B. Fiorini, K. Koyama and T. Baker, *Fast production of cosmological emulators in modified gravity: the matter power spectrum*, *JCAP* **12** (2023) 045, [[2310.05786](#)].
- [64] H. T. Jense, I. Harrison, E. Calabrese, A. Spurio Mancini, B. Bolliet, J. Dunkley et al., *A complete framework for cosmological emulation and inference with CosmoPower*, *RAS Tech. Instrum.* **4** (2025) rzaf002, [[2405.07903](#)].
- [65] S. Trusov, P. Zarrouk and S. Cole, *Neural network-based model of galaxy power spectrum: fast full-shape galaxy power spectrum analysis*, *Mon. Not. Roy. Astron. Soc.* **538** (2025) 1789–1799, [[2403.20093](#)].
- [66] J. Bai and J.-Q. Xia, *FREmu: Power Spectrum Emulator for $f(R)$ Gravity*, *Astrophys. J.* **971** (2024) 11, [[2405.05840](#)].
- [67] N. Kaushal, E. Giusarma and M. Reyes, *nuGAN: Generative Adversarial Emulator for Cosmic Web with Neutrinos*, [2505.03936](#).
- [68] I. Mohammed and U. Seljak, *Analytic model for the matter power spectrum, its covariance matrix, and baryonic effects*, *Mon. Not. Roy. Astron. Soc.* **445** (2014) 3382–3400, [[1407.0060](#)].

- [69] H. Winther, S. Casas, M. Baldi, K. Koyama, B. Li, L. Lombriser et al., *Emulators for the nonlinear matter power spectrum beyond Λ CDM*, *Phys. Rev. D* **100** (2019) 123540, [[1903.08798](#)].
- [70] B. Bose, M. Tsedrik, J. Kennedy, L. Lombriser, A. Pourtsidou and A. Taylor, *Fast and accurate predictions of the non-linear matter power spectrum for general models of Dark Energy and Modified Gravity*, *Mon. Not. Roy. Astron. Soc.* **519** (2023) 4780–4800, [[2210.01094](#)].
- [71] D. J. Bartlett, L. Kammerer, G. Kronberger, H. Desmond, P. G. Ferreira, B. D. Wandelt et al., *A precise symbolic emulator of the linear matter power spectrum*, *Astron. Astrophys.* **686** (2024) A209, [[2311.15865](#)].
- [72] C. Sui, D. J. Bartlett, S. Pandey, H. Desmond, P. G. Ferreira and B. D. Wandelt, *syren-new: Precise formulae for the linear and nonlinear matter power spectra with massive neutrinos and dynamical dark energy*, *Astron. Astrophys.* **698** (2025) A1, [[2410.14623](#)].
- [73] PARTICLE DATA GROUP collaboration, S. Navas et al., *Review of particle physics*, *Phys. Rev. D* **110** (2024) 030001.
- [74] PLANCK collaboration, N. Aghanim et al., *Planck 2018 results. VI. Cosmological parameters*, *Astron. Astrophys.* **641** (2020) A6, [[1807.06209](#)].
- [75] DESI collaboration, W. Elbers et al., *Constraints on Neutrino Physics from DESI DR2 BAO and DR1 Full Shape*, [2503.14744](#).
- [76] SUPERNOVA SEARCH TEAM collaboration, A. G. Riess et al., *Observational evidence from supernovae for an accelerating universe and a cosmological constant*, *Astron. J.* **116** (1998) 1009–1038, [[astro-ph/9805201](#)].
- [77] DESI collaboration, A. G. Adame et al., *DESI 2024 VI: cosmological constraints from the measurements of baryon acoustic oscillations*, *JCAP* **02** (2025) 021, [[2404.03002](#)].
- [78] X. Chen, M.-x. Huang, S. Kachru and G. Shiu, *Observational signatures and non-Gaussianities of general single field inflation*, *JCAP* **01** (2007) 002, [[hep-th/0605045](#)].
- [79] G. Jung, M. Citran, B. van Tent, L. Dumilly and N. Aghanim, *Constraints on primordial non-Gaussianity from Planck PR4 data*, [2504.00884](#).
- [80] P. D. Meerburg, M. Münchmeyer, J. B. Muñoz and X. Chen, *Prospects for Cosmological Collider Physics*, *JCAP* **03** (2017) 050, [[1610.06559](#)].
- [81] D. Karagiannis, A. Lazanu, M. Liguori, A. Raccanelli, N. Bartolo and L. Verde, *Constraining primordial non-Gaussianity with bispectrum and power spectrum from upcoming optical and radio surveys*, *Mon. Not. Roy. Astron. Soc.* **478** (2018) 1341–1376, [[1801.09280](#)].
- [82] F. Villaescusa-Navarro, C. Hahn, E. Massara, A. Banerjee, A. M. Delgado, D. K. Ramanah et al., *The Quijote Simulations*, *Astrophys. J. Supp.* **250** (Sept., 2020) 2, [[1909.05273](#)].
- [83] V. Springel, *The Cosmological simulation code GADGET-2*, *Mon. Not. Roy. Astron. Soc.* **364** (2005) 1105–1134, [[astro-ph/0505010](#)].
- [84] M. D. McKay, R. J. Beckman and W. J. Conover, *A comparison of three methods for selecting values of input variables in the analysis of output from a computer code*, *Technometrics* **21** (1979) 239–245.
- [85] A. Lewis, A. Challinor and A. Lasenby, *Efficient computation of CMB anisotropies in closed FRW models*, *Astrophys. J.* **538** (2000) 473–476, [[astro-ph/9911177](#)].
- [86] M. Zennaro, J. Bel, F. Villaescusa-Navarro, C. Carbone, E. Sefusatti and L. Guzzo, *Initial Conditions for Accurate N-Body Simulations of Massive Neutrino Cosmologies*, *Mon. Not. Roy. Astron. Soc.* **466** (2017) 3244–3258, [[1605.05283](#)].
- [87] W. R. Coulton, F. Villaescusa-Navarro, D. Jamieson, M. Baldi, G. Jung, D. Karagiannis et al., *Quijote-PNG: Simulations of primordial non-Gaussianity and the information content of the*

matter field power spectrum and bispectrum, *arXiv e-prints* (June, 2022) arXiv:2206.01619, [2206.01619].

- [88] G. Jung, D. Karagiannis, M. Liguori, M. Baldi, W. R. Coulton, D. Jamieson et al., *Quijote-PNG: Quasi-maximum Likelihood Estimation of Primordial Non-Gaussianity in the Nonlinear Dark Matter Density Field*, *Astrophys. J.* **940** (Nov., 2022) 71, [2206.01624].
- [89] R. Scoccimarro, *Transients from initial conditions: a perturbative analysis*, *Mon. Not. Roy. Astron. Soc.* **299** (1998) 1097, [astro-ph/9711187].
- [90] M. Crocce, S. Pueblas and R. Scoccimarro, *Transients from Initial Conditions in Cosmological Simulations*, *Mon. Not. Roy. Astron. Soc.* **373** (2006) 369–381, [astro-ph/0606505].
- [91] K. Pearson, *Liii. on lines and planes of closest fit to systems of points in space*, *The London, Edinburgh, and Dublin Philosophical Magazine and Journal of Science* **2** (1901) 559–572.
- [92] A. V. Dorogush, V. Ershov and A. Gulin, *Catboost: gradient boosting with categorical features support*, 2018.
- [93] T. Chen and C. Guestrin, *Xgboost: A scalable tree boosting system*, in *Proceedings of the 22nd ACM SIGKDD International Conference on Knowledge Discovery and Data Mining*, KDD '16, (New York, NY, USA), p. 785–794, Association for Computing Machinery, 2016, DOI.
- [94] G. Ke, Q. Meng, T. Finley, T. Wang, W. Chen, W. Ma et al., *Lightgbm: A highly efficient gradient boosting decision tree*, in *Advances in Neural Information Processing Systems* (I. Guyon, U. V. Luxburg, S. Bengio, H. Wallach, R. Fergus, S. Vishwanathan et al., eds.), vol. 30, Curran Associates, Inc., 2017.